PCCP

Comparing the Structures and Photophysical Properties of Two Charge Transfer Co-crystals

Journal:	*Physical Chemistry Chemical Physics*
Manuscript ID	CP-ART-08-2023-003720.R1
Article Type:	Paper
Date Submitted by the Author:	11-Sep-2023
Complete List of Authors:	Abou Taka, Ali; Sandia National Laboratories California, Reynolds III, Joseph; Sandia National Laboratories California Cole-Filipiak, Neil; Sandia National Laboratories California, Combustion Research Facility Shivanna, Mohana; Sandia National Laboratories California Yu, Christine J.; Northwestern University Feng, Patrick; Sandia National Laboratories California Allendorf, Mark; Sandia National Laboratories California Ramasesha, Krupa; Sandia National Laboratories California, Gas Phase Chemical Physics Stavila, Vitalie; Sandia National Laboratories California, Engineered Materials Department, MS-9161 McCaslin, Laura; Sandia National Laboratories California, Combustion Research Facility

PCCP

Comparing the Structures and Photophysical Properties of Two Charge Transfer Co-crystals

Received 00th January 20xx,
Accepted 00th January 20xx

DOI: 10.1039/x0xx00000x

Ali Abou Taka, [a] Joseph E. Reynolds III, [a] Neil C. Cole-Filipiak, [a] Mohana Shivanna, [a] Christine J. Yu, [b] Patrick Feng, [a] Mark D. Allendorf, [a] Krupa Ramasesha, [a] Vitalie Stavila, [a] and Laura M. McCaslin[a*]

Organic co-crystals have emerged as a promising class of semiconductors for next-generation optoelectronic devices due to their unique photophysical properties. This paper presents a joint experimental-theoretical study comparing the crystal structure, spectroscopy, and electronic structure of two charge transfer co-crystals. Reported herein is a novel co-crystal Npe:TCNQ, formed from 4-(1-naphthylvinyl) pyridine (Npe) and 7,7,8,8-tetracyanoquinodimethane (TCNQ) via molecular self-assembly. This work also presents a revised study of the co-crystal composed of Npe and 1,2,4,5-tetracyanobenzene (TCNB) molecules, Npe:TCNB, herein reported with a higher-symmetry (monoclinic) crystal structure than previously published. Npe:TCNB and Npe:TCNQ dimer clusters are used as theoretical model systems for the co-crystals; the geometries of the dimers are compared to geometries of the extended solids, which are computed with periodic boundary conditions density functional theory. UV-Vis absorption spectra of the dimers are computed with time-dependent density functional theory and compared to experimental UV-Vis diffuse reflectance spectra. Both Npe:TCNB and Npe:TCNQ are found to exhibit neutral character in the S_0 state and ionic character in the S_1 state. The high degree of charge transfer in the S_1 state of both Npe:TCNB and Npe:TCNQ is rationalized by analyzing the changes in orbital localization associated with the S_1 transitions.

1 Introduction

In the search for semiconducting materials with tailored optoelectronic properties, organic co-crystals have emerged as particularly promising for applications in integrated photonics, photovoltaic devices, and organic LEDs.[1-14] Co-crystals are crystalline, single-phase materials composed of two or more molecular compounds that interact noncovalently.[3] One class of these, charge transfer (CT) co-crystals, can be defined by CT interactions between molecular subunits of electron donor and acceptor molecules.[3] Organic CT co-crystals are particularly interesting for the development of optoelectronic devices, exhibiting behaviors such as ambipolar charge transport,[3,5,6] tunable emission,[7-9] and room temperature ferroelectricity.[2,10]

There are significant challenges to finding combinations of donors and acceptors that produce co-crystals with properties such as long exciton lifetimes. Researchers use the principles of rational design to identify structure-function relationships to correlate properties of individual molecules to the properties of bulk materials.[3,11-14] High-throughput screening and machine learning methods are also commonly used to identify candidate materials.[15-19] These methods screen combinations of donor and acceptor molecules to predict materials' bulk physical properties from molecular metrics based on geometric and energetic parameters.[20,21] Machine learning and high-throughput screening approaches rely on fundamental studies of materials that employ

[a] Sandia National Laboratories, Livermore, California 94550, USA
[b] Department of Chemistry, Northwestern University, Evanston, Illinois 60208, USA
†Electronic Supplementary Information (ESI) available

crystal structure determination, spectroscopic characterization, and electronic structure characterization.

In this work we present a comparative study of the structural and photophysical properties of two D-A co-crystals: 4-(1-naphthylvinyl)pyridine (Npe) co-crystalized with 1,2,4,5-tetracyanobenzene (TCNB) and Npe co-crystalized with 1,2,4,5-tetracyanoquinodimethane (TCNQ), shown in Figure 1. We report a revised crystallographic study of Npe:TCNB, in which we find a monoclinic crystal structure, in contrast to the previously reported triclinic structure.[22] A crystal structure of the second system studied here, Npe:TCNQ, has not been reported to date; we thus present the first studies of the structure and photophysical properties of Npe:TCNQ. Theoretically, the S_0 optimized geometries of the D-A dimer models are computed using density functional theory (DFT). Dimer geometries are compared to calculations of the crystal structures, computed with periodic boundary conditions (PBC) DFT, to assess structural differences arising from the constraints of the extended solid. We benchmark our DFT methods and choice of dimer conformer by comparing experimental crystal and theoretical dimer UV-Vis spectra. We report the degree of CT in the ground (S_0) and first electronically excited singlet state (S_1) of our theoretical dimer models and rationalize these values by computing the degree of electronic localization change between the S_1 transition orbitals of the D-A complexes using a recently developed metric.[21]

2 Methods Section

2.1 Computational Methods

2.1.1 Methodology

A variety of DFT methods and basis sets were benchmarked and used to identify possible minimum energy structures along the neutral Npe:TCNB and Npe:TCNQ dimer potential energy surfaces (PESs), with additional information given in ESI Tables S1-S2. Geometry optimizations and relative energies were computed and compared using functionals ωB97X-D, B3LYP, B3LYP-D3, CAM-B3LYP, CAM-B3LYP-D3, and M06-2X and basis sets 6-31G(d,p), 6-31+G(d,p), and 6-311+G(d,p), resulting in 18 combinations of functional and basis set.[23–30] Here, a D3 suffix on the functional name refers to the Grimme D3 dispersion correction, needed for the calculation of non-covalent bonding interactions.[30] We find that CAM-B3LYP-D3/6-31+G(d,p) calculations of the dimer clusters best reproduce the geometries found in the experimental crystal structures and UV-Vis spectra without the need for any long-range parameter tuning. In the search for local minima on the dimer PESs, guess dimer geometries were generated by extracting the donor-acceptor subunit geometry from the experimental crystal structure and rotating the donor relative to the acceptor, keeping the π stacking motif intact. Small increments in rotation angle between the donor and acceptor (2°) enabled an exhaustive search of relevant conformers. Geometry optimizations of theoretical crystal structures were performed with periodic boundary conditions (PBC) DFT using the hybrid functional HSE06 and 6-31G(d,p) basis; the experimental crystal structure geometries were used as initial guesses.[27-29,31] Hybrid functionals such as HSE06 combine semi local exchange and non-local Hartree-Fock exchange, yielding improved band gaps, excitation energies, and thermochemical properties compared to those computed with pure functionals (see Ref. 32 and references within). Minimum structures were obtained by optimizing all coordinates and unit cell lengths using an energy convergence criterion of 10^{-5}. The number of k points used for Npe:TCNB is 28 and for Npe:TCNQ, 36. Direct band gaps are reported using these PBC DFT parameters. Excited state calculations were carried out using CAM-B3LYP-D3/6-31+G(d,p) within the linear response time–dependent DFT (TDDFT) formalism, with additional details given in ESI, Tables S3-S12 and Figures S14-23.[33-35] Natural bond orbital (NBO) population analysis[36] has been shown to perform well in quantifying the degree of CT in donor-acceptor systems[37-39] and is used here to analyze S_0 CT in the complexes. Transition density matrix (TDM) analysis was used to calculate the degree of CT in the S_1 states using Theodore, which has been shown to reliably quantify S_1 CT.[21,40] Excited state analysis was facilitated by Martin's Natural Transition Orbital (NTO) model.[41]

All calculations described in 2.1.1 were carried out using the GAUSSIAN suite of electronic structure programs, G16.[42] The computed UV-Vis spectra reported in Figures 7a and 10a are gaussian broadened with standard deviation σ = 0.2 eV using the UV-Vis plotting tool in G16.[42] Stability was tested on all converged Kohn–Sham determinants.[43] Stationary points were verified as minima using harmonic frequency analysis, employing analytical second–derivative calculations.[44] All relative energies of structures are zero-point energy corrected, employing the harmonic approximation. See ESI Tables S1-S2 for more details.

Calculations of the changes to orbital localization in the S_1 transitions are performed as suggested in Ref. 21. Orbital localization is quantified by computing the integral overlap between donor HOMO and D-A dimer HOMO, as well as acceptor LUMO and D-A dimer LUMO, which we refer to as orbital similarity. These orbital similarity values range between 0 (no similarity) and 1 (same orbital). Donor and acceptor geometries are taken to be the geometries they assume in the optimized D-A dimer complex (i.e. donor and acceptor geometries are not geometric minima of the isolated molecules), allowing for the simplification that the overlap matrix of atomic basis functions between donor and D-A complex (as well as acceptor and D-A complex) is equivalent to the self-overlap of atomic basis functions, reported in the output of our electronic structure calculations.[21]

2.2 Experimental Methods

2.2.1 General Comments

All co-crystals were synthesized in ambient conditions. 1,2,4,5-tetracyanoquinodimethane (TCNQ) was purchased from Acros Chemical and used as received. 1,2,4,5-tetracyanobenzene (TCNB) and 4-(1-naphthylvinyl)pyridine (Npe) were purchased from TCI America and used as received. All organic solvents were purchased from Sigma-Aldrich and used as received.

2.2.2 General Instrumentation

Powder X-ray Diffraction (PXRD): Patterns for the bulk powders were collected with a Panalytical Empyrean Diffractometer system equipped with a PIXcel3D detector using CuKα radiation using

samples loaded in glass capillaries (Charles Supper, Inc.) and sealed with vacuum grease. See Figures 5a, 8.

Single Crystal X-Ray Crystallography (SCXRD): Suitable crystals were mounted on a thin glass fiber using perfluoropolyether oil, which was frozen in situ by a nitrogen gas cryostream flow. Data collection was performed on a Rigaku Super Nova diffractometer equipped with an AtlasS2 CCD, and Oxford 700 low-temperature attachment, using CuKα (λ = 1.54184). Using Olex2, structures were solved with the SHELX structure solution program using Direct Methods and refined with the SHELXL refinement package using least squares minimization. See additional details in ESI, Figures S1-S9 and ESI Section 3.

Fourier Transform Infrared (FTIR): Spectra were obtained with an Agilent Cary-630 spectrometer, with an attenuated total reflectance module containing a diamond crystal. See additional info in ESI, Figures S10-S11.

Elemental Microanalyses: Elemental microanalyses were performed by Galbraith Laboratories, Inc. (Knoxville, TN).

Photoluminescence (PL) Spectroscopy: Photoluminescence spectra were collected using an Edinburgh Instruments FLS1000 fluorimeter equipped with a 450 W Xenon arc lamp for steady-state measurements and a 375 nm picosecond pulsed light emitting diode for time-resolved measurements. Single-grating Czerny-Turner excitation and emission monochromators were used along with a cooled PMT-900 photomultiplier detector that covers a range of 185-900 nm. Absorption spectra were collected between 300-540 nm monitoring the emission at a wavelength of 550 nm. Emission spectra were collected between 424-740 nm with an excitation wavelength of 375 nm. See Figure 5b-c.

2.2.3 Synthesis of Npe:TCNB co-crystals

Npe:TCNB co-crystals were synthesized by dissolution of 0.5 mmol TCNB and 0.5 mmol Npe in a 20 mL vial with 6 mL of a 1:1 DMF:MeCN solvent. Once fully dissolved, the yellow solution was allowed to slowly evaporate forming broad needle-like crystals. Bulk powder form of the Npe:TCNB co-crystals can be formed by the mixing of two separate TCNB and Npe solutions in pure MeCN.

2.2.4 Synthesis of Npe:TCNQ co-crystals

Npe:TCNQ co-crystals were synthesized by dissolution of 0.15 mmol of Npe and 0.1 mmol of TCNQ, combined in a 7 mL vial with 4 mL of MeCN and heated/boiled until all solids were dissolved. This resulted in a dark green solution, forming small blue-like plates as it slowly cooled to room-temperature overnight. (Note: the crystallographic ratio is the opposite of the synthesis conditions). Further purification and isolation were achieved by washing with cold MeCN.

2.2.5 Diffuse Reflectance Spectra

UV-Vis and near-IR spectra of solid Npe, TCNB, TCNQ, Npe:TCNB, and Npe:TCNQ were acquired in diffuse reflectance mode using a Perkin-Elmer Lambda 1050+ spectrophotometer. Samples were finely ground and mixed with MgO powder (~40 µm particle size) to make ~1 wt.% mixtures. Sample mixtures were then pressed against a CaF_2 window mounted onto the side of a 100 mm integrating sphere.

2.2.6 Band Gap Determination

To compute the optical band gap of each co-crystal, the diffuse reflectance spectra shown in Figures 7b, 10b were first transformed using the Kubelka-Munk transformation.[45] The resulting *F(R)* spectra were treated as pseudo-absorption functions, assuming the scattering coefficients are constant for small spectral windows near the onset of the lowest energy feature. In this approximation, the linear portion of plots of $F(R)^{1/\gamma}$ *vs*. photon energy were extrapolated to the x-axis to determine the optical band gap.[46] For direct band gap materials, such plots appear linear for γ = 1/2 whereas indirect band gap materials show good linearity for γ = 2. *F(R)* plots for both materials, along with linear extrapolations, are presented in ESI, Figures S12-S13. As none of these *F(R)* plots show obvious improvements in linearity, we report the direct band gap. Due to the vibronic structure observed in Npe:TCNQ, multiple linear fits were performed up to the lowest energy shoulder at ~862 nm.

3 Results and Discussion

Dimer cluster geometries are optimized to determine a low-energy conformer before properties such as orbital energies and vibrational frequencies are calculated. We perform detailed benchmarking of (1) the level of theory/basis set, and (2) the comparison between theoretical and experimental spectroscopic data to validate our methods and models.

In this section we compare two D-A co-crystal systems with commonly used donor and acceptor molecules. These two co-crystal systems employ the same donor molecule, Npe, and structurally similar acceptors, TCNB and TCNQ. The first acceptor, TCNB, has been used in the synthesis of co-crystals with applications in waveguides and photoswitching devices.[22,47,48] The second acceptor, TCNQ, is one of the most widely studied acceptor species due to its high electron affinity (EA).[6,49-52] Co-crystals with a TCNQ acceptor are known for strong CT character and some exhibit room temperature ambipolar charge transport.[6,47-52] While Npe:TCNB co-crystals have recently been of interest in the development of waveguides for integrated photonics,[22] to the authors' knowledge, Npe:TCNQ co-crystals have not been reported to date

3.1 Comparing Orbital Overlap and Charge Transfer of Npe:TCNB and Npe:TCNQ

We performed scans of the PESs of Npe:TCNB and Npe:TCNQ using CAM-B3LYP-D3/6-31+G(d,p) with additional details in Section 2.1.1. Figures 2 and 3 show the minimum geometries identified for each system. Our tests of the recently developed orbital similarity metric are performed on the lowest-energy isomer for each system.[21] Additional benchmarking to confirm the chosen models is described in Sections 3.2-3.3.

Figure 4 presents the HOMO and LUMO isosurfaces and orbital energies of Npe, TCNB, TCNQ, Npe:TCNB, and Npe:TCNQ. One of the most striking features of the orbital isosurfaces is the similarity of the Npe:acceptor complexes' HOMO and Npe HOMO isosurfaces, as well as those of the Npe:acceptor complexes' LUMO and acceptor LUMO. Because a large degree of CT is observed in the S_1 states (HOMO→LUMO) of each complex, we analyze the change

in orbital localization by computing the similarity of the dimer cluster orbitals to the donor and acceptor molecular orbitals using a recently developed method,[21] as shown in Table 1. In the case of Npe:TCNB, we find an average similarity of 0.99 between the Npe HOMO and Npe:TCNB HOMO (Npe-Npe:TCNB) and TCNB LUMO and Npe:TCNB LUMO (TCNB-Npe:TCNB). In the case of Npe:TCNQ, we find an average similarity of 0.98 between the Npe HOMO and Npe:TCNQ HOMO (Npe-Npe:TCNQ) and TCNQ LUMO and Npe:TCNQ LUMO (TCNQ-Npe:TCNQ). Our explicit calculations of the degree of CT in S_1 (see Figures 2 & 3) reveal a high degree of CT in both complexes, with 0.97e in the S_1 state of Npe:TCNB and 0.95e in the S_1 state of Npe:TCNQ. The differences in orbital similarity between Npe:TCNB and Npe:TCNQ are quite small, as reflected by small differences in the degree of S_1 CT between the two systems.

We now turn to comparing orbital energies using well-established techniques. Prior studies have used the metric E_{HOMO}^{donor}-$E_{LUMO}^{acceptor}$ to identify the degree of CT in the ground state, with larger values of E_{HOMO}^{donor}-$E_{LUMO}^{acceptor}$ representing higher values of S_0 CT.[20] The energy difference between isolated Npe HOMO and TCNB LUMO (E_{HOMO}^{Npe}-E_{LUMO}^{TCNB}) is (-7.02 eV) – (-3.04 eV) = -3.98 eV. In the Npe and TCNQ orbital analysis, we observe an E_{HOMO}^{Npe}-E_{LUMO}^{TCNQ} difference of (-7.02 eV) – (-3.98 eV) = -3.04 eV. Comparing the E_{HOMO}^{Npe}-$E_{LUMO}^{acceptor}$ values between the two systems, we observe that E_{HOMO}^{Npe}-E_{LUMO}^{TCNQ} = −3.04 eV is higher than E_{HOMO}^{Npe}-E_{LUMO}^{TCNB} = −3.98 eV, indicating a slightly larger degree of S_0 CT.

We can also compare the orbital energies between Npe:TCNB and Npe:TCNQ using an analysis based on Koopman's theorem to assess the degree of S_0 CT, estimating that the EA is approximately equal to the negative of the LUMO energy. This gives an EA^{TCNB} of 3.04 eV vs. an EA^{TCNQ} of 3.98 eV. Correlating the estimations of EA to calculations of S_0 CT, we observe that Npe:TCNB exhibits a slightly smaller degree of CT, 0.02e, compared to 0.04e in Npe:TCNQ, as one would expect from TCNB's smaller EA.

3.2 Structural and Electronic Characterization of Npe:TCNB

We now turn to detailed benchmarking of our model systems against experimental crystal structures and spectroscopic data. As briefly described in 3.1, we performed scans of the S_0 PES of the Npe:TCNB dimer and identified six structures as candidate dimer models for the extended solids, shown in Figure 2. A previous study identified two low-energy minimum geometries of the Npe:TCNB dimer.[22] In the six conformers identified here, two agree with the previously reported geometries by Zhu et al., including the lowest-energy isomer, a. We find that multiple minima exist upon rotation of TCNB with respect to the naphthalene of Npe (see Section 2.1), resulting in our identification of two low-energy structures that differ in energy by 0.009 eV (b) and 0.062 eV (c), respectively, from the lowest-energy structure (a). We also identify a structure at 0.107 eV for which TCNB is localized to the pyridine of the Npe (d). The highest energy structure (0.179 eV, f) found in this study is structurally similar to the higher energy structure determined by Zhu et al.[22] Finally, a folded structure with relative energy 0.111 eV (e) was identified. In this structure, the Npe molecule is folded in a V-shape and TCNB is localized at the naphthalene moiety. Further analysis of the structures can be found in Section 2.1 in the ESI.

To compare our model dimer structure to the experimental crystal structure, Npe:TCNB co-crystals were synthesized and spectroscopically characterized. Single crystals of Npe:TCNB were grown by slow evaporation of a 1:1 molar ratio of TCNB and Npe dissolved in a 1:1 (vol.) DMF/MeCN mixture, resulting in yellow blade-like crystals suitable for single-crystal X-ray diffraction (SCXRD). Analysis by SCXRD determined that the Npe:TCNB co-crystal, in contrast to the previously reported triclinic structure,[22] crystallizes with a 1:1 ratio of TCNB to Npe in the monoclinic space group P21/c with a = 6.73, b = 36.66, and c = 9.51 Å(β = 106◦). Although the single-crystal XRD measurement was performed at 100 K, there is still a large amount of disorder around the pyridine moiety of Npe, which appears to be "rocking" and generating an additional conformation of the pyridine ring that is >45◦ out of the plane with respect to the other occupied pyridine site. The expanded structure reveals that there is a π – π stacking interaction between the naphthalene moiety of the Npe and the benzene ring of the TCNB molecule with a distance of 3.375 Å. The pyridine of Npe interacts with other Npe-pyridines in adjacent layers with a centroid-centroid distance of 3.9 – 4.9 Å, Figure S4. The crystal structure shows no evidence of interaction between the Npe pyridine moiety and TCNB. Further details on the crystal structure data are given in ESI Section 3.

Steady-state and time-resolved photoluminescence measurements were collected on Npe:TCNB co-crystals to further probe the interactions between the Npe and TCNB moieties, as shown in Figures 5b and 5c. The emission spectra show a single peak centered near 550 nm, which is red shifted ∼ 0.7 eV from that of Npe itself, centered near 425 nm.[22] This shift is associated with CT interactions between Npe and TCNB.[53] The observed fluorescence decay for Npe:TCNB follows a bi-exponential decay with decay components of 2.43 ns (14.6%) and 9.54 ns (85.4%). These values differ from that of pure Npe (1.57 ns)[53] and reflect appreciable electronic interactions in the excited state between the two co-crystal components.

PBC DFT calculations were carried out to study the effects of the extended solid on the geometry of the unit cell and found to be in agreement with the both the experimental crystal structure and dimer model, shown in Figure 6. Due to the significant computational expense of PBC DFT calculations, we can only compute ground state geometries and energies. We thus focus our comparison between ground state PBC DFT and dimer calculations. Two main structural differences are observed in the comparison between the PBC DFT structure and its dimer counterpart. First is the alignment of the TCNB molecule relative to Npe. The dimer structure exhibits a -14.5° rotation of the TCNB, while the PBC DFT structure exhibits a 2.0° rotation, and experimental crystal structure a 3.3° rotation. Another key difference is the planarity of Npe observed in the structures, calculated as the dihedral between the pyridine and naphthalene moieties. This dihedral angle is 2.8° in the PBC DFT structure and 13.3° in the dimer structure, compared to the 2.0° in the experimental crystal structure. While we see

larger differences between the dimer geometry and experimental crystal structure compared to the PBC DFT geometry, the dimer structures exhibit the key qualitative features of the crystal structure. Some geometric differences between PBC DFT and dimer structures are to be expected, as the crystal structure constrains the structures of the D-A pairs. We thus turn to assess the importance of these structural differences via comparisons of the experimental UV-Vis spectra and theoretically predicted UV-Vis spectra of the dimer cluster.

While we have strong structural and energetic arguments for our choice of the optimal dimer model of Npe:TCNB, we must compare the computed UV-Vis absorption spectra to the experimental UV-Vis diffuse reflectance spectra, shown in Figure 7 a-b. Here we compare dips in the experimental reflectance spectra to calculated absorption peaks. The exact % R peak shapes will not be examined closely, as features such as >100% R values shown at low wavelength are likely due to fluorescence emission and outside the scope of this discussion. The calculated S_1 state at 430 nm with oscillator strength f = 0.021 a.u. is characterized by a HOMO→LUMO transition, originating from intermolecular CT from Npe to TCNB, as shown in Figure 7. This transition corresponds to the experimentally observed dip around 450 nm (Figure 7). The peak computed at 310 nm corresponds to the S_4 excited state, f = 0.478, seen experimentally at 350 nm. In contrast to the CT character of the S_1 state, the S_4 state exhibits local excitation within Npe, as seen in Figure 7c. The theoretical S_{10} peak, f =0.356, computed at 250 nm (in excellent agreement with the experimental dip at 250 nm), is characterized by two orbital transitions, both with locally excited character, shown in Figure 7c. The good agreement between the simulated spectrum of the cluster model and the experimental diffuse reflectance spectrum of the crystals supports our choice of the lowest-energy cluster model.

The UV-Vis diffuse reflectance spectra were analyzed to determine the band gap of Npe:TCNB crystals, as described in Section 2.2.6. The direct band gap is determined to be 2.45 eV. Our PBC DFT calculations determine the direct band gap to be 2.03 eV. The inherent challenges to using PBC DFT to compute accurate band gaps are well documented. However, hybrid functionals, such as the one used in this study, balance local and non-local exchange, resulting in computed band gaps that compare better with experimental values than those computed with other functionals (see Ref. 32 and references within). We thus find reasonable agreement between the PBC DFT and experimentally derived direct band gaps, especially given the theoretical challenges.

3.3 Structural and Electronic Characterization of Npe:TCNQ

We now turn to studying the electronic structure, crystal structure, and UV-Vis spectra of Npe:TCNQ. We performed scans of the PES of the Npe:TCNQ dimer to identify structures of the model cluster that best reproduce the crystal structure. Figure 3 shows the optimized minimum-energy structures located on the Npe:TCNQ dimer PES. Four low-energy dimer structures were identified with a 0.029 eV energy gap between the lowest and the highest energy structure. The four conformers differ from each other by the rotation of the TCNQ with respect to the naphthalene moiety, with significant rotations seen in conformers b and c, labeled in Figure 3. Further analysis of the structures can be found in Section 2.2 in the ESI.

To ensure that the lowest-energy conformer of Npe:TCNQ is the closest in structure to a D-A subunit in the extended solid, crystals of Npe:TCNQ were synthesized and characterized. Single crystals of the Npe:TCNQ co-crystal were grown by slowly cooling a warm solution of TCNQ and Npe dissolved in MeCN at 330 K. This resulted in precipitation of large dark blue prismatic crystals. Analysis by SCXRD determined that the Npe:TCNQ crystallizes with a 2:3 ratio in the triclinic space group P-1 with cell parameters of a = 9.88, b = 11.81, c = 12.31 Å, α = 93.8◦, β = 93.94◦, and γ = 111.87◦. The crystal structure reveals layers of TCNQ and Npe alternating in pairs similar to that of the Npe:TCNB co-crystal as shown in Figures S1-S9 of the ESI. The stacking of the layers displays a pair of TCNQ molecules interacting with a single Npe molecule from an adjacent layer. The close proximity of the layers enables a π − π stacking interaction between the naphthalene moiety of the Npe with one TCNQ (3.730 Å) and an interaction with a second TCNQ and the pyridine moiety of the Npe (3.841 Å). Despite the close interactions between TCNQ and Npe within the same layer, the distance between the two interlayer Npe pyridine moieties is too large (4.847 Å) for substantial π – π interaction. Further details on the crystal structure data are given in ESI Section 3.

Photoluminescence measurements were attempted for the Npe:TCNQ system, though no detectable fluorescence was observed. We attribute the fluorescence quenching to self-absorption effects.[54]

PBC DFT calculations were performed to quantify the effects of the extended solid on the structure of the D–A subunit in the crystal. Figure 9 shows that the PBC DFT calculated structure is in good agreement with the experimentally observed structure with a centroid-centroid distance difference of 0.21 Å between experiment and PBC DFT. The main differences between the PBC and dimer structures are: 1) the degree of rotation of TCNQ with respect to Npe and 2) the centroid-centroid distances. There is a significant degree of rotation observed in the dimer structure (54.8°) compared to that of the experimental crystal structure (-5.7°), whereas the rotation in the PBC structure differs from the experimental crystal structure by only 2.8°. Although a high degree of rotation is observed in the dimer structure, the centroid-centroid distance exhibits only a small deviation from the experimental crystal structure, 0.05 Å, compared to the distance deviation between the PBC DFT structure and experiment, 0.21 Å. Due to the significant differences between dimer and crystal structure, we turn to comparing the theoretical and experimental UV-Vis spectra to validate the dimer model.

The UV-Vis absorption spectra of the Npe:TCNQ dimer were calculated, shown in Figure 10a. The simulated spectrum of Npe:TCNQ shows a peak at 660 nm, associated with the S_1 excited state. This state corresponds to a CT state, with electronic density moving from the Npe to the TCNQ (HOMO→LUMO), as shown in Figure 10c. The S_1 state has an oscillator strength of f = 0.0299 a.u. This peak is observed experimentally within the vibronic structure region between 600 and 900 nm. Two additional peaks in the calculated spectrum are located at 440 and 380 nm, associated with

excited states S_2 and S_4, respectively. S_2 has an oscillator strength of f = 0.310 a.u. and for S_4, 0.280 a.u. Both states exhibit mixed character between locally excited and CT transitions, with local excitation originating mainly from the TCNQ $\pi \rightarrow \pi*$ transition. These peaks likely correspond to the less intense dip observed in the experimental spectrum at 420 nm. A final strong peak at 320 nm originates from the S_8 excited state with strong oscillator strength, f = 0.860 a.u., aligning with the observed experimental dip at 340 nm. This excitation is characterized by the intramolecular Npe $\pi \rightarrow \pi*$ transition; see Figure 10c. Similar vibronic structure observed between 600 and 900 nm in other co-crystals has been attributed to formation of radical anion pairs of TCNQ and donor.[55-56]

The UV-Vis diffuse reflectance spectra were analyzed to determine the band gap in the Npe:TCNQ crystals, as described in Sections 2.2.6 and 3.2. A direct band gap is determined to be 1.38 eV. Our PBC DFT calculations determine the direct band gap to be 0.79 eV. In the case of Npe:TCNQ, PBC DFT and experimental band gaps do not agree as nicely as in the case of Npe:TCNB, but still fall within typical deviations for hybrid functionals.[32]

4 Conclusions

The availability of accurate crystal structures of CT co-crystal complexes is essential for developing chemical databases for materials discovery. To this aim we report details of the syntheses and crystal structures of Npe:TCNB and Npe:TCNQ co-crystals. Our reinvestigation of the crystal structure of Npe:TCNB reveals a monoclinic structure, previously assigned as triclinic.[22] High-resolution crystal structures are necessary for benchmarking theoretical models and quantifying the structural effects of crystal packing on dimer subunits. Experimental UV-Vis diffuse reflectance spectra were measured to assess the peak positions and intensities of bright states of the co-crystals. Comparing relative intensities of these states to those calculated for theoretical molecular model systems plays an integral role in assessing the quality of our D-A dimer models. Furthermore, experimental UV-Vis diffuse reflectance spectra of Npe:TCNQ reveal vibronic structure in the 600-900 nm region, indicating strong photon-induced CT. Analysis of the S_0 states of the model clusters reveals that the degree of S_0 CT is slightly greater in Npe:TCNQ than in Npe:TCNB, as predicted differences in EA. We employ a novel metric for quantifying changes in orbital localization to rationalize the large degree of S_1 CT in each system.[21] We find that differences in the S_0 and S_1 degree of CT in each system are quite small, with each system exhibiting dominantly neutral character in the S_0 state and ionic character in the S_1 state. The joint experimental-theoretical methodology presented here for quantifying ground and excited state CT in CT co-crystals enables high-accuracy benchmarking of models for future discovery of novel co-crystals with desired optoelectronic properties such as long exciton lifetimes.

Author Contributions

A.A.T. performed the calculations and analysis and co-wrote the manuscript. J.E.R. synthesized the crystals and aided in characterization. N.C.C-F. performed UV-Vis diffuse reflectance spectroscopy and provided insights into spectral assignments. M.S. aided in characterization of the co-crystals. C.J.Y. aided in synthesizing and characterizing the co-crystals. P.F. aided in performing the photoluminescence experiments. M.A. provided insights on the connection of this work with the greater literature. K.R. aided in performing UV-Vis diffuse reflectance spectroscopy, provided insights into spectral assignments, and made connections with the literature. V.S. proposed study of the Npe:TCNQ, aided in synthesis of the crystals, aided in characterization of the crystals, and provided insights into connecting to the literature. L.M.M. aided in performing calculations and analysis of the orbital similarity and co-wrote the manuscript. All authors contributed to the interpretation of the results.

Conflicts of interest

There are no conflicts to declare.

Acknowledgements

The authors would like to thank Dr. Shinae Kim for her comments on the manuscript and Dr. Kevin Carter-Fenk for discussions on PBC DFT. This work is supported by the Laboratory Directed Research and Development program at Sandia National Laboratories. Sandia National Laboratories is a multi-mission laboratory managed and operated by National Technology & Engineering Solutions of Sandia, LLC (NTESS), a wholly owned subsidiary of Honeywell International Inc., for the U.S. Department of Energy's National Nuclear Security Administration (DOE/NNSA) under contract DE-NA0003525. This written work is authored by an employee of NTESS. The employee, not NTESS, owns the right, title and interest in and to the written work and is responsible for its contents. Any subjective views or opinions that might be expressed in the written work do not necessarily represent the views of the U.S. Government. The publisher acknowledges that the U.S. Government retains a non-exclusive, paid-up, irrevocable, world-wide license to publish or reproduce the published form of this written work or allow others to do so, for U.S. Government purposes. The DOE will provide public access to results of federally sponsored research in accordance with the DOE Public Access Plan.

Notes and references

1. K. P. Goetz, D. Vermeulen, M. E. Payne, C. Kloc, L. E. McNeil and O. D. Jurchescu, J. Mater. Chem. C, 2014, 2, 3065–3076.
2. S. Horiuchi, F. Ishii, R. Kumai, Y. Okimoto, H. Tachibana, N. Nagaosa and Y. Tokura, Nat. Mater., 2005, 4, 163–166.
3. L. Sun, Y. Wang, F. Yang, X. Zhang and W. Hu, Adv. Mater., 2019, 31, 1902328.
4. S. K. Park, J. H. Kim and S. Y. Park, Adv. Mater., 2018, 30, 1704759.
5. C. Wang, H. Dong, W. Hu, Y. Liu and D. Zhu, Chem. Rev., 2012, 112, 2208–2267.
6. J. Zhang, H. Geng, T. S. Virk, Y. Zhao, J. Tan, C.-A. Di, W. Xu, K. Singh, W. Hu, Z. Shuai, Y. Liu and D. Zhu, Adv. Mater., 2012, 24, 2603–2607.

7. S. Li, Y. Lin and D. Yan, J. Mater. Chem. C, 2016, 4, 2527–2534.
8. P. Majumdar, F. Tharammal, J. Gierschner and S. Varghese, ChemPhysChem, 2020, 21, 616–624.
9. W. Jiang, X. Ma, D. Liu, G. Zhao, W. Tian and Y. Sun, Dyes Pigm., 2021, 193, 109519.
10. Z. Wang and Q. Zhang, Asian J. Org. Chem., 2020, 9, 1252–1261.
11. L. Sun, W. Zhu, F. Yang, B. Li, X. Ren, X. Zhang and W. Hu, Phys. Chem. Chem. Phys. 2018, 20, 6009–6023.
12. D. Yan and D. G. Evans, Mater. Horiz., 2014, 1, 46–57.
13. H.-D. Wu, F.-X. Wang, Y. Xiao and G.-B. Pan, J. Mater. Chem. C, 2014, 2, 2328–2332.
14. Y. Huang, Z. Wang, Z. Chen and Q. Zhang, Angew. Chem., 2019, 58, 9696–9711.
15. A. Mahmood and J.-L. Wang, Energy Environ. Sci., 2021, 14, 90–105.
16. Y. Wu, J. Guo, R. Sun and J. Min, Npj Comput. Mater., 2020, 6, 1–8.
17. S. A. Lopez, B. Sanchez-Lengeling, J. de Goes Soares and A. Aspuru-Guzik, Joule, 2017, 1, 857–870.
18. X. Liu, Y. Shao, T. Lu, D. Chang, M. Li and W. Lu, Mater. Des., 2022, 216, 110561.
19. P. Malhotra, J. C. Verduzco, S. Biswas and G. D. Sharma, ACS Appl. Mater. Interfaces, 2022.
20. W. Shi, T. Deng, Z. M. Wong, G. Wu and S.-W. Yang, Npj Comput. Mater., 2021, 7, 1–8.
21. A. Abou Taka, J. M. Herbert and L. M. McCaslin, ChemRxiv, 2023, DOI: 10.26434/chemrxiv-2023-1xz7b.
22. W. Zhu, L. Zhu, Y. Zou, Y. Wu, Y. Zhen, H. Dong, H. Fu, Z. Wei, Q. Shi and W. Hu. Adv. Mater., 2016, 28, 5954–5962.
23. J.-D. Chai and M. Head-Gordon, Phys. Chem. Chem. Phys., 2008, 10, 6615–6620.
24. A. Becke, The quantum theory of atoms in molecules: from solid state to DNA and drug design, John Wiley & Sons, 2007.
25. T. Yanai, D. P. Tew and N. C. Handy, Chem. Phys. Lett., 2004, 393, 51–57.
26. Y. Zhao and D. G. Truhlar, Theor. Chem. Acc., 2008, 120, 215–241.
27. P. C. Hariharan and J. A. Pople, Theor. Chim. Acta, 1973, 28, 213–222.
28. M. J. Frisch, J. A. Pople and J. S. Binkley, J. Chem. Phys., 1984, 80, 3265–3269.
29. K. Raghavachari, J. S. Binkley, R. Seeger and J. A. Pople, J. Chem. Phys., 72 (1980) 650-54.
30. S. Grimme, S. Ehrlich and L. Goerigk, J. Comput. Chem., 2011, 32, 1456–1465.
31. J. Heyd and G. E. Scuseria, J. Chem. Phys., 2004, 121, 1187–1192.
32. E. N. Brothers, A. F. Izmaylov, J. O. Normand, V. Barone and G. Scuseria, J. Chem. Phys., 2008, 129, 011102.
33. R. Bauernschmitt and R. Ahlrichs, Chem. Phys. Lett., 1996, 256, 454–464.
34. M. E. Casida, C. Jamorski, K. C. Casida and D. R. Salahub, J. Chem. Phys., 1998, 108, 4439–4449.
35. R. E. Stratmann, G. E. Scuseria and M. J. Frisch, J. Chem. Phys., 1998, 109, 8218–8224.
36. E. D. Glendening, A. E. Reed, J. E. Carpenter and F. Weinhold, The NBO3.0 Program, 2001, University of Wisconsin, Copyright.
37. A.E. Reed, L. A. Curtiss, F. Weinhold, Chem. Rev., 1988, 88, 899-926.
38. P. Verma, A. Srivastava, P. Tandon, M. R. Shimpi, Front. Chem., 2022, 10, 855132.
39. P. Prajapati, J. Pandey, P. Tandon, K. Sinha, M. R. Shimpi, Front. Chem., 2022, 10, 848014.
40. F. Plasser. "TheoDORE: A toolbox for a detailed and automated analysis of electronic excited state computations." J. Chem. Phys. 2020, 152, 084108.
41. R. L. Martin, J. Chem. Phys., 2003, 118, 4775–4777.
42. M. J. Frisch, G. W. Trucks, H. B. Schlegel, G. E. Scuseria, M. A. Robb, J. R. Cheeseman, G. Scalmani, V. Barone, G. A. Petersson, H. Nakatsuji, X. Li, M. Caricato, A. V. Marenich, J. Bloino, B. G. Janesko, R. Gomperts, B. Mennucci, H. P. Hratchian, J. V. Ortiz, A. F. Izmaylov, J. L. Sonnenberg, D. Williams-Young, F. Ding, F. Lipparini, F. Egidi, J. Goings, B. Peng, A. Petrone, T. Henderson, D. Ranasinghe, V. G. Zakrzewski, J. Gao, N. Rega, G. Zheng, W. Liang, M. Hada, M. Ehara, K. Toyota, R. Fukuda, J. Hasegawa, M. Ishida, T. Nakajima, Y. Honda, O. Kitao, H. Nakai, T. Vreven, K. Throssell, J. A. Montgomery, Jr., J. E. Peralta, F. Ogliaro, M. J. Bearpark, J. J. Heyd, E. N. Brothers, K. N. Kudin, V. N. Staroverov, T. A. Keith, R. Kobayashi, J. Normand, K. Raghavachari, A. P. Rendell, J. C. Burant, S. S. Iyengar, J. Tomasi, M. Cossi, J. M. Millam, M. Klene, C. Adamo, R. Cammi, J. W. Ochterski, R. L. Martin, K. Morokuma, O. Farkas, J. B. Foresman and D. J. Fox, Gaussian 16 Revision B.01, 2016, Gaussian Inc. Wallingford CT.
43. R. Seeger and J. A. Pople, J. Chem. Phys., 1977, 66, 3045–3050.
44. H. F. Schaefer III and Y. Yamaguchi, J. Mol. Struct.: THEOCHEM , 1986, 135, 369–390.
45. P. Kubelka and F. Munk, "An Article on Optics of Paint Layers", Z. Tech. Phys. 12, 1931, 593–603.
46. J. I. Pankove, Courier Dover Publications, New York, NY, 1971, Ch. Absorption, pp. 34–52.
47. L. Y. Long, L. S. Liao and S. T. Lee, J. Am. Chem. Soc., 2013, 135, 3744-3747.
48. Z. Weigang, R. Zheng, X. Fu, H. Fu, Q. Shi, Y. Zhen, H. Dong and W. Hu, Angew. Chem. Int. Ed., 2015, 54, 6785-6789.
49. I. Shokaryev, A. Buurma, O. Jurchescu, M. Uijttewaal, G. De Wijs, T. Palstra and R. A. de Groot, J. Phys. Chem. A, 2008, 112, 2497–2502.
50. W. Zhu, Y. Yi, Y. Zhen, and W. Hu, Small, 2015, 11, 2150–2156.
51. A. Bandrauk, K. Truong and C. Carlone, Can. J. Chem., 1982, 60, 588–595.
52. D. Vermeulen, L. Zhu, K. Goetz, P. Hu, H. Jiang, C. Day, O. Jurchescu, V. Coropceanu, C. Kloc and L. McNeil, J. Phys. Chem. C, 2014, 118, 24688–24696.
53. S. Li and D. Yan, Adv. Opt. Mater., 2018, 6, 1800445.
54. Mechanisms and Dynamics of Fluorescence Quenching, ed. J. R. Lakowicz, Springer US, Boston, MA, 2006, pp. 331–351.
55. H. T. Jonkman and J. Kommandeur, Chem. Phys. Lett., 1972, 15, 496–499.
56. I. Haller and F. Kaufman, J. Am. Chem. Soc., 1976, 98, 1464–1468.

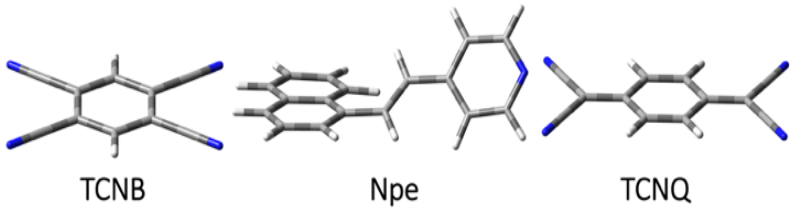

Figure 1: Structures of TCNB, Npe, and TCNQ

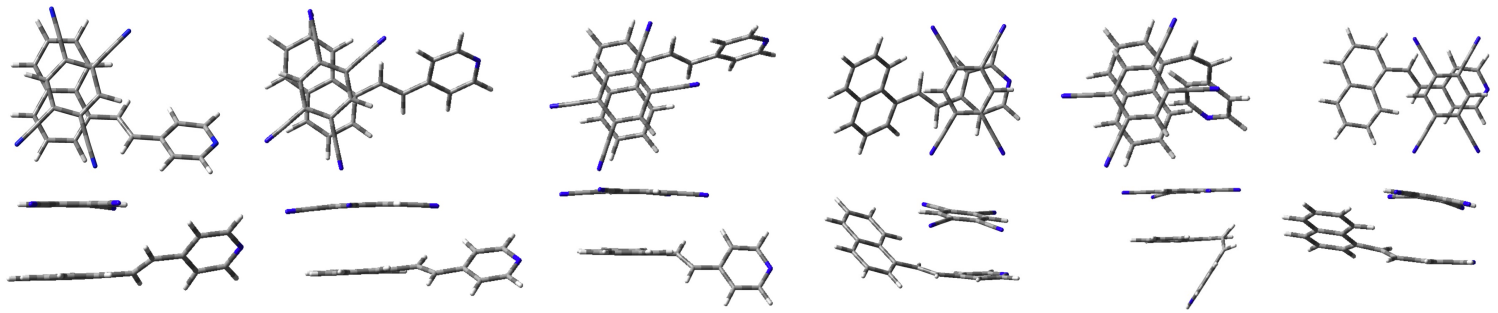

		a	b	c	d	e	f
Energy$_{rel}$ (eV)		**0.000**	**0.009**	**0.062**	**0.107**	**0.111**	**0.179**
Degree of CT (e)	**S_0**	**0.02**	**0.02**	**0.02**	**0.01**	**0.02**	**0.01**
	S_1	**0.97**	**0.97**	**0.97**	**0.98**	**0.96**	**0.98**
Osc. Strengths (au)		**0.021**	**0.003**	**0.009**	**0.016**	**0.023**	**0.002**

Figure 2: Optimized geometries of Npe:TCNB found with CAM-B3LYP-D3/6-31+G(d,p). Energies (eV) are reported relative to the lowest-energy structure (a) and include zero-point energy corrections. The calculated degree of CT is reported for S_0 and S_1, as well as the associated S_0-S_1 oscillator strengths.

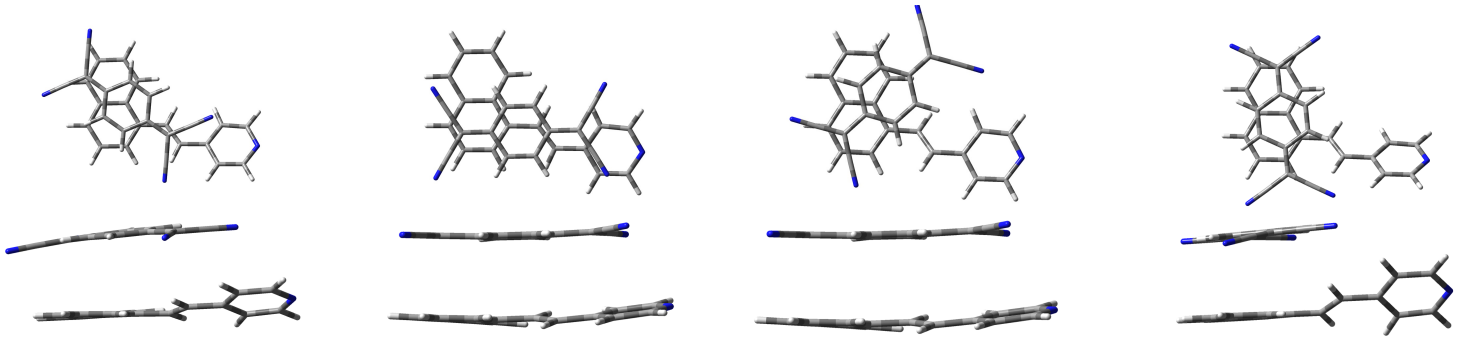

		a	b	c	d
Energy$_{rel}$ (eV)		**0.000**	**0.010**	**0.026**	**0.029**
Degree of CT (e)	**S_0**	**0.04**	**0.07**	**0.04**	**0.01**
	S_1	**0.88**	**0.82**	**0.90**	**0.97**
Osc. Strengths (au)		**0.030**	**0.065**	**0.026**	**0.002**

Figure 3: Optimized geometries of Npe:TCNQ found with CAM-B3LYP-D3/6-31+G(d,p). Energies (eV) are reported relative to the lowest-energy structure (a) and include zero-point energy corrections. The calculated degree of CT is reported for S_0 and S_1, as well as the associated S_0-S_1 oscillator strengths.

	Npe-Npe:TCNB (HOMO)	TCNB-Npe:TCNB (LUMO)	Npe-Npe:TCNQ (HOMO)	TCNQ-Npe:TCNQ (LUMO)
Orbital Similarity	0.99	0.99	0.98	0.98
Average Similarity	0.99		0.98	

Table 1: Values of the orbital similarity metric are reported for each system along with the average similarity value.

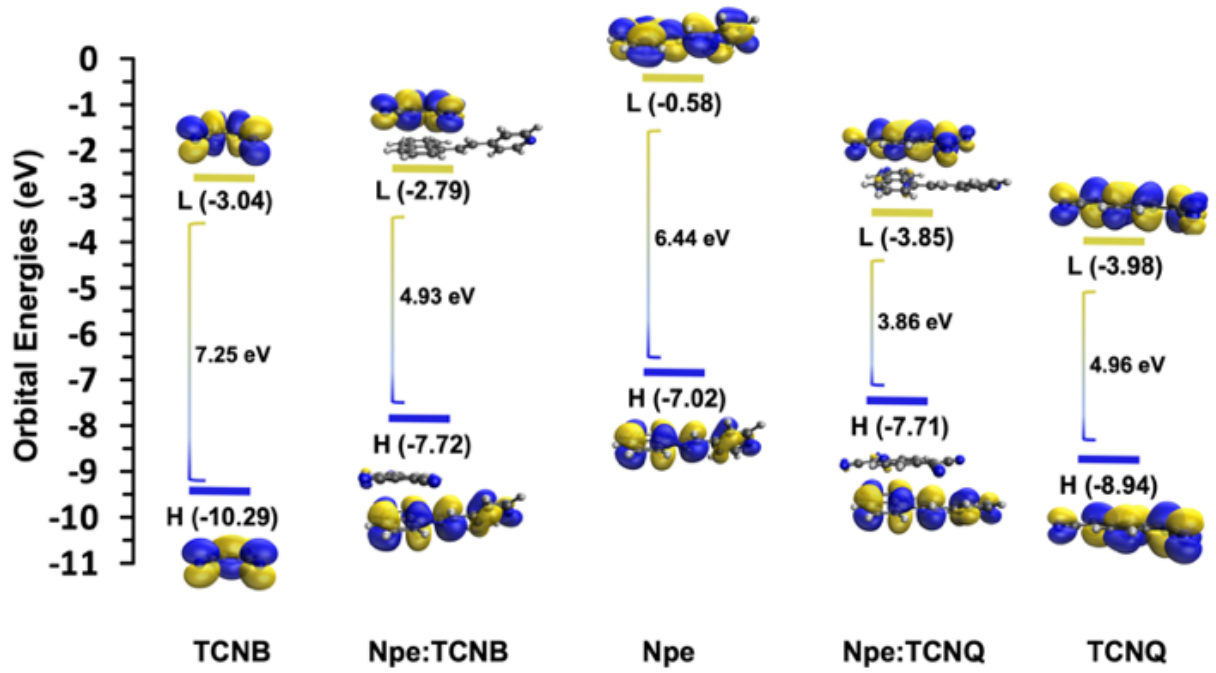

Figure 4: The molecular orbital energy level diagram for Npe:TCNQ and Npe:TCNB complexes with their isolated molecules. Orbital energy gaps are also shown. Orbitals are plotted with isovalue of 0.05 $Å^{-3}$.

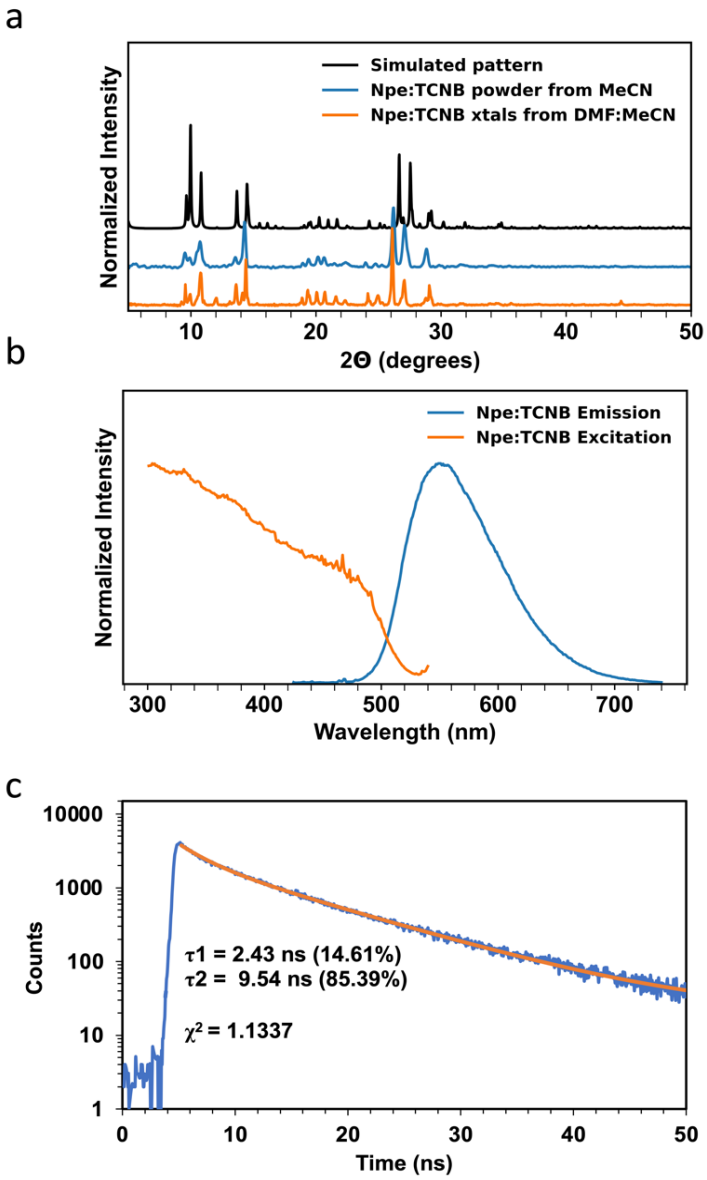

Figure 5: a) Powder X-ray patterns of Npe:TCNQ obtained from simulation of the crystal structure (top trace), MeCN (middle trace), and by DMF/MeCN (bottom trace). b) The absorption and PL spectra of Npe:TCNB co-crystals on a glass substrate at 298 K. c) The PL decay profile (with fitting curve).

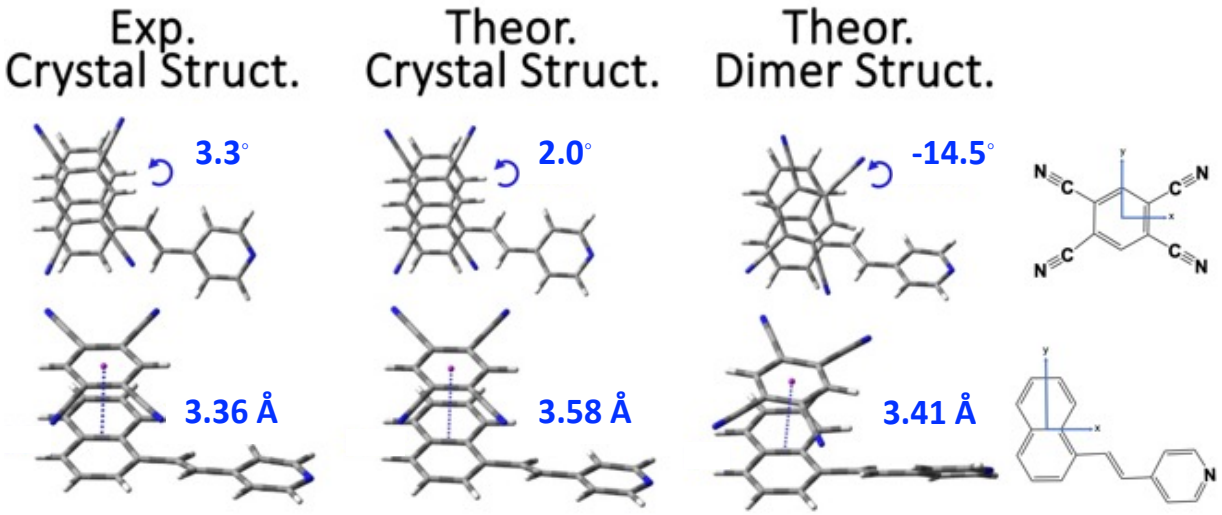

Figure 6: Geometries of Npe:TCNB from the experimental crystal structure (left), theoretical crystalline structure (center), and theoretical dimer structure (right), with centroid-centroid distances indicated with dotted line.

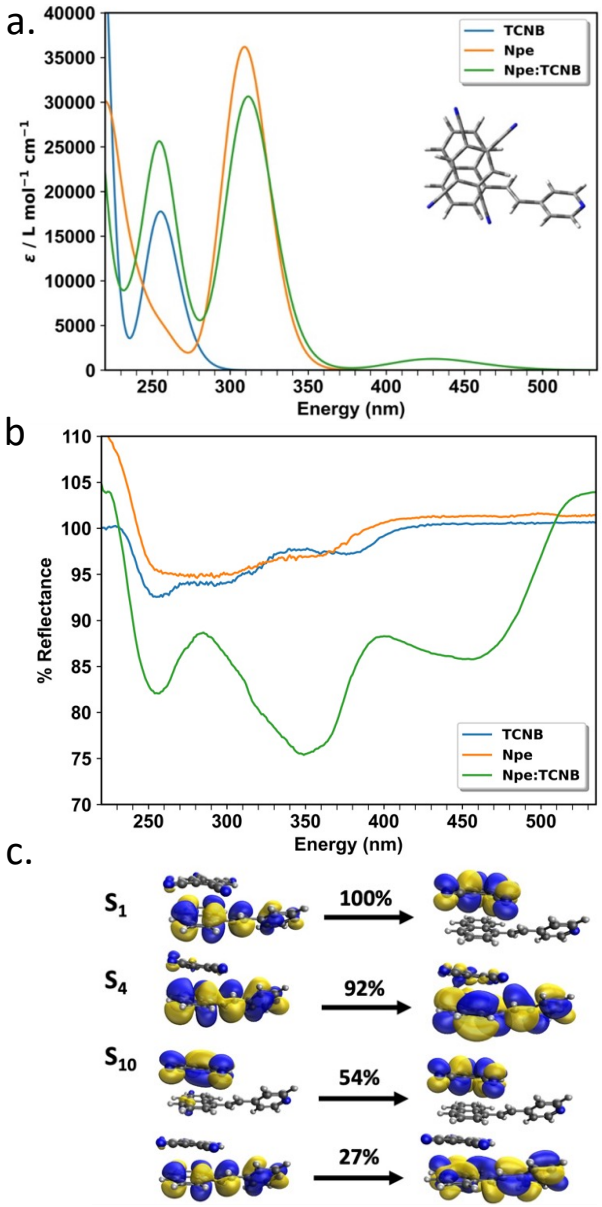

Figure 7: a) The simulated absorption spectra of Npe, TCNB, and Npe:TCNB in the dimer. b) Diffuse reflectance spectra of ~1 wt.% mixtures of Npe, TCNB, and Npe:TCNB. c) Orbital contributions of strong electronic transitions and their associated weights.

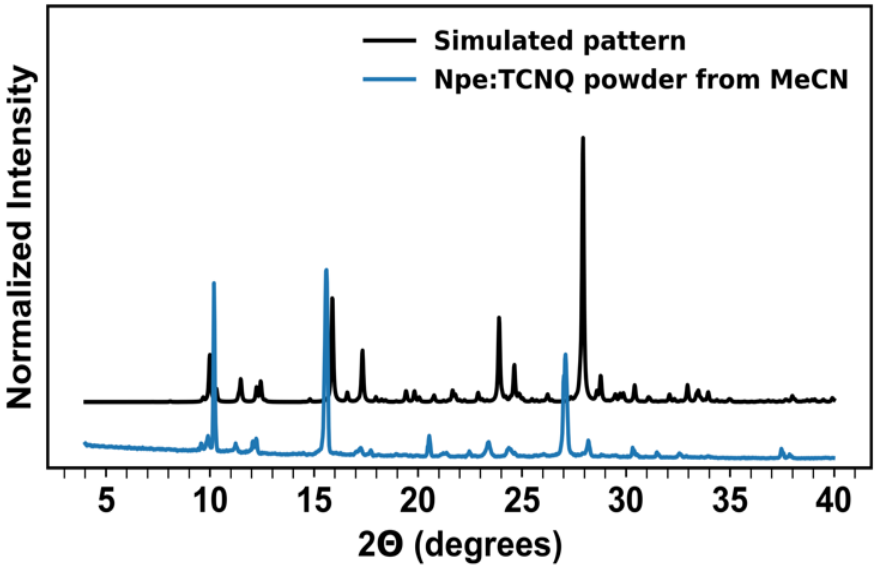

Figure 8: Powder X-ray patterns of Npe:TCNQ (bottom trace) and simulated from the crystal structure (top trace).

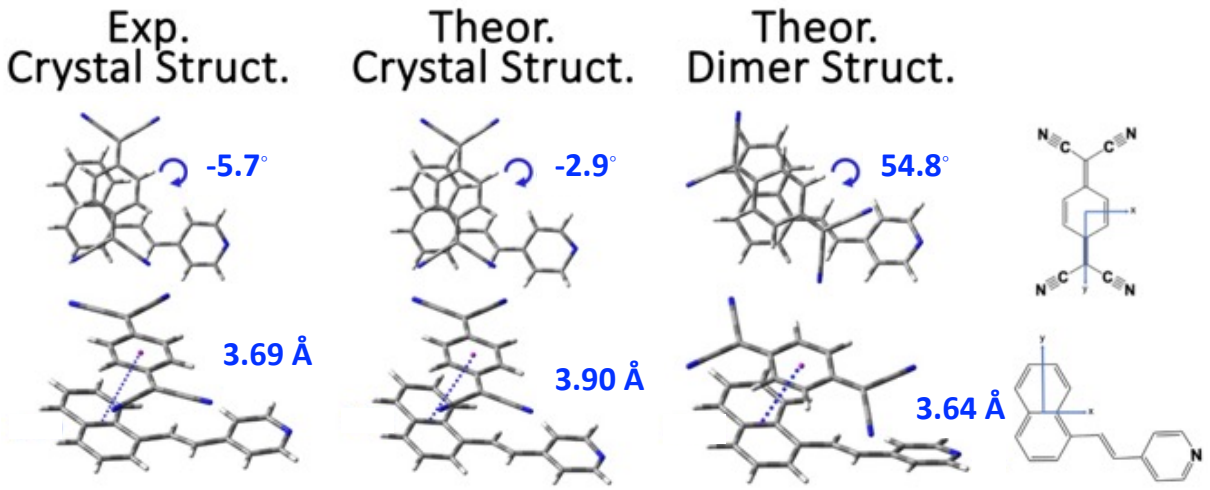

Figure 9: Geometries of Npe:TCNQ from the experimental crystal structure (left), theoretical crystalline structure (center), and theoretical dimer structure (right), with centroid-centroid distances indicated with dotted line.

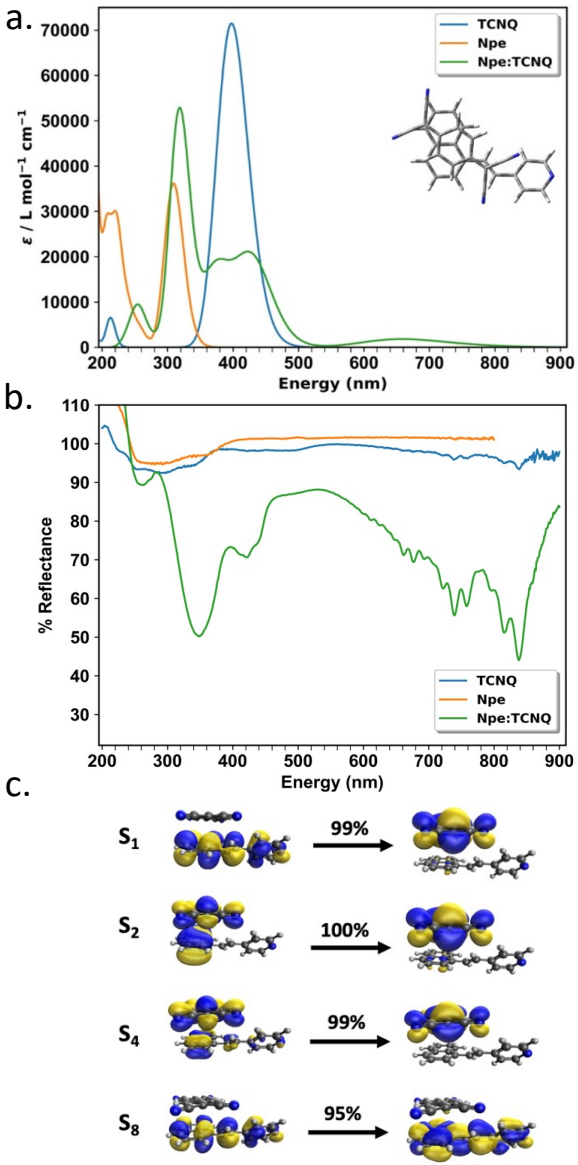

Figure 10: a) The simulated absorption spectra of Npe, TCNQ, and Npe:TCNQ in the dimer. b) Diffuse reflectance spectra of Npe, TCNQ, and Npe:TCNQ in MgO. c) Orbital contributions of strong electronic transitions and their associated weights.